Physico-chemical characterisation and tribological behaviour of ground micro-arc oxidation coating on aluminium alloy – Comparison with hard anodised oxidation

Louis Rodriguez, Aurélien Vieu, Marion Balsarin, Philippe Combes, Joël Alexis, Jérôme Esvan, Samuel Lesko, Jean Denape, Jean-Yves Paris, Karl Delbé

Highlights

Physico-chemical characterisation and tribological behaviour of micro-arc oxidation coating on aluminium alloy – Comparison with hard anodised oxidation

Louis Rodriguez, Aurélien Vieu, Marion Balsarin, Philippe Combes, Joël Alexis, Jérôme Esvan, Samuel Lesko, Jean Denape, Jean-Yves Paris, Karl Delbé

- MAO coating is made of $\alpha-$, $\gamma-$alumina, aluminosilicate and amorphous silica ;
- MAO mechanical properties are about three times higher than those of the HA coating ;
- The best wear resistance condition on was the ground MAO coating.

Physico-chemical characterisation and tribological behaviour of micro-arc oxidation coating on aluminium alloy – Comparison with hard anodised oxidation

Louis Rodriguez[a,b], Aurélien Vieu[a], Marion Balsarin[b], Philippe Combes[b], Joël Alexis[a], Jérôme Esvan[c], Samuel Lesko[d], Jean Denape[a], Jean-Yves Paris[a] and Karl Delbé[a,*]

[a]Laboratoire Génie de Production (LGP), Université de Toulouse, INP-ENIT, 47 avenue d'Azereix, Tarbes, 65000, Occitanie, France
[b]Galvanoplastie Industrielle Toulousaine, 7 rue J-M Jacquard, Cugnaux, 31270, Occitanie, France
[c]CIRIMAT, Université de Toulouse, INP-ENSIACET, , 4 allée Emile Monso, Toulouse, 31030, Occitanie, France
[d]Bruker Nano Surface Metrology Division, 7 rue de la Croix Martre, Palaiseau, 91120, Île-de-France, France

ARTICLE INFO

Keywords:
Aluminium coating
Plasma electrolytic oxidation
Sliding wear
Third body

ABSTRACT

This study aims to compare the tribological properties of classical hard anodisation (HA) and a ground micro-arc oxidation (MAO) coating. Analysis on MAO showed that its hardness and elastic modulus are around three times greater than HA. Wear tests were evaluated using a linearly reciprocating ball-on-flat using alumina balls. The HA coating did not withstand the test. The substrate was severely degraded. MAO coating wear rate is 3.1×10^{-5} $mm^3 \cdot N^{-1} \cdot m^{-1}$. It is 22 times lower than that on HA coating. Energy dissipated calculation showed that 26 kJ is needed to remove 1 mm^3 of materials from MAO tribocouple. Conversely, only 0.7 kJ is needed to remove 1 mm^3 from HA tribocouple.

1. Introduction

The use of innovative solutions would reduce the energy lost due to friction and wear by around 40% in 15 years (1). Because of its low density and abundance, aluminium, the most widely used non-ferrous metal globally, remains important in reducing the overall mass of the systems and the energy consumed to operate them. However, its low hardness makes it sensitive to abrasive wear if not protected by any surface treatment. Various processes have been developed to increase the surface hardness of aluminium parts. Hard chromium is a particularly effective coating where hardness between 900 and 1000 HV can be achieved (2). However, it is not compatible with REACH regulations. HA is the most common treatment for improving the wear resistance of aluminium parts (3). It allows obtaining a hardness in the range of 450 to 600 HV. Moreover, it is REACH compliant as long as it is not sealed in a potassium dichromate bath. Finally, micro-arc oxidation (MAO) is a promising REACH compliant anodic surface treatment process designed to limit wear.

Micro-arc oxidation (MAO) is also refered in the literature to Plasma Electrolytic Oxidation (PEO) (4) and to Anodic Spark Deposition (ASD) (5). This technique uses a high potential difference, usually alternating or pulsed at a frequency varying between 100 Hz and 1000 Hz, a high electrical potential (400 to 1000 V) and a very high current density between the workpiece and a counter electrode. Mechanism of formation of such layer is a succession of oxide dielectric breakdown, fusion and crystallisation (6).

When a barrier-type oxide layer reaches a certain thickness, dielectric breakdown occurs and ends the "normal" growth of the oxide (7). The breakdown of the anodic layer is characterised by a "breakdown voltage" (U_B) accompanied by a visible spark and an audible snap. The breakdown voltage usually depends on the type of metal being anodised and the electrolyte composition and resistivity. However, it is independent of the current density, temperature, surface topography and the stirring speed of the electrolyte (8). The intense electric fields cause a local rise in the oxide

*Corresponding author
louis.rodriguez@git.fr (L. Rodriguez); aurelienvieu31@gmail.com (.A. Vieu); marion.balsarin@git.fr (.M. Balsarin); philippe.combes@git.fr (.P. Combes); Joel.alexis@enit.fr (.J. Alexis); jerome.esvan@toulouse-inp.fr (.J. Esvan); samuel.lesko@bruker.com (.S. Lesko); jean.denape@enit.fr (.J. Denape); jean-yves.paris@enit.fr (.J. Paris); karl.delbe@enit.fr (.K. Delbé)
ORCID(s): 0000-0002-8974-3462 (L. Rodriguez); 0000-0001-8137-3770 (.A. Vieu); 0000-0002-6769-6124 (.J. Alexis); 0000-0002-0496-9447 (.J. Denape); 0000-0002-1562-935X (.J. Paris); 0000-0002-8503-2671 (.K. Delbé)

Alloy elements	Mg	Fe	Mn	Si	Zn	Cr	Ti	Cu	Al
Concentration (%)	3.5 - 4.5	0.5	0.2 - 0.7	0.4	0.25	0.05 - 0.25	0.15	0.1	base

Table 1
Chemical composition (weight percent) of an aluminium alloy 5086 H111 (32).

R_m (MPa)	$R_{p0.2}$ (MPa)	A (%)	Hardness (HBW)
240 - 310	mini 100	15	65

Table 2
Mechanical properties of an aluminium alloy 5086 H111 (33).

temperature by Joule effect. The low density of charge carriers causes the formation of micro-arcs. The voltage (or electric field) required for the oxide breakdown depends on the passive layer thickness.

The application of an intense electric field increases the speed of movement of the ions and thus intensifies the accumulation of heat. When the electric field exceeds the critical value of the breakdown voltage, the oxide structure becomes sufficiently disordered that ions can pass directly through the disordered oxide structure rather than through gaps. This change causes atoms and ions to collide in the oxide layer, resulting in micro-arcs. Indeed, as the thickness of the oxide layer increases, the equivalent resistance of the system increases and therefore, the required breakdown voltage also increases (9).

The layers obtained are thick (up to 500 µm (10)), have a significant adhesion with the substrate and are recognised for their high mechanical properties. As this technique causes the formation of an electrolytic plasma discharge to produce an oxide layer (6). It can be used for most valve metals and their alloys (11; 12; 13).

Layers formed on the aluminium surface are ceramic types and consist of a dense inner layer and a friable outer layer. The dense inner layer is around 60-70% of the total thickness layer. In most applications, a grinding process removes the friable outer layer. The aim is to reduce the roughness and remove the brittle layer to obtain the most friction-friendly surface and avoid abrasive particle circulation in the tribological system. Characteristics provided to the surfaces make aluminium parts attractive for a wide range of tribological and wear applications. Different tribological test configurations were set up to study the friction properties of these coatings. These tests can be grouped into different categories: linear reciprocating (14; 15; 16; 17), ball on disc (15; 18; 19; 20; 21; 22; 23), ball on alternative disc (5), block-on-ring (24), abrasion (24; 25). The tribological properties of a couple of materials are dependent on numerous factors. In particular, the sliding materials are surrounded by the experimental system which has its own mechanical and vibrating behavior, and are separated by interfacial elements such as the detached particles (from the contacting surfaces) which strongly affect the friction and wear results (26; 27; 28). This study then proposes to compare HA and ground MAO coatings under conditions as close as possible. The tests were carried out on the same tribometer and under the same friction conditions. Thus, it was possible to construct two tribological circuits illustrating the different flows of matter to compare the frictional and wear behaviours of the material pairs under conditions as close as possible. It is therefore essential to test both HA and MAO coatings under the same conditions to compare their properties. A few studies have done this work (14; 29; 30). Some have also studied the effect in friction properties of polished surfaces (14; 15; 18). However, no work has been proposed to study the effect of mechanical grinding on tribological properties.

This study is the first to provide a tribological comparison between hard anodizing and ground micro-arcs oxidation coatings as used in the industry.

Finally, for the first time to the author's knowledge, a tribological circuit describing the frictional behaviour of the first two bodies is proposed for both the HA coating and the ground MAO coating.

2. Material manufacturing and characterisation

The different treatments are performed on 5086 aluminium alloy plates. The composition and mechanical properties of the alloy are given in the Tables 1 and 2. The metallurgical condition H111 means that the alloy has been annealed and slightly hardened (31). The treated specimens are square plates of 100 mm side and 4 mm thickness.

2.1. Hard anodisizing process

Hard anodising (HA) is an anodising treatment for obtaining thick oxide coatings on aluminium substrates. This technique is commonly used to improve the wear resistance of aluminium parts. Conventional anodising treatment is always preceded by several operations known as pre-treatment. The first step of the preparation consists of degreasing in a commercial solution of Bonderite 4215 NC-LT. Then a basic etching is carried out in a basic solution composed of sodium hydroxide and sodium glucoheptonate. Finally, an immersion in a nitric acid bath is carried out as a last preparation step to remove the alloying elements concentrated on the surface. The aqueous electrolyte has a concentration of 225 ± 25 g/L in sulphuric acid. It is refrigerated at 0 ± 5 °C. The current density used is about 2.5 ± 0.5 A/dm^2. The thickness of the HA layers produced for this study is 55 ± 5 µm.

2.2. Micro-arc oxidation process

Micro-arc oxidation treatments are carried out at Galvanoplastie Industrielle Toulousaine (GIT) through CERATRONIC process (34) using the company production installation. The treatment tank contains 900 L of electrolyte and is maintained at a temperature of 23 °C by a cooling unit. The production generator CERATRONIC (CER325) is connected to the workpiece and its 316L steel counter-electrode. The electrolyte consists of 5.4 g/L of liquid sodium silicate concentrated at 1.37 kg/L and 1 g/L of potassium hydroxide diluted in deionised water. Finally, the bath must have a conductivity of $\sigma = 3 \pm 1.5$ mS.cm^{-1} and a pH = 11 ± 1.5.

The treatment chosen as a reference for the study of the MAO coating and its tribological properties follow the conditions mastered by the company.

The treatment is divided into three-time sequences of variable parameters, and the total duration of the process is 70 min. Plates are treated in pairs, and only one face is treated for each. The thickness of the MAO layers is 110 ± 10 µm. Finally, a finish grinding is done with a diamond wheel, and 50% of the total thickness is removed. In this way, the ground surface is located in the dense layer.

2.3. Microstructure and surface analysis of the coatings

Observations on HA and ground MAO coatings cross-sections show that both coatings have good adhesion to the substrate. Thicknesses are measured at five different points for each cross-sectional view. The thickness measured on HA is 52 ± 1 µm [Figure 1.a]. The one obtained on the ground MAO is 58 ± 1 µm [Figure 1.b].

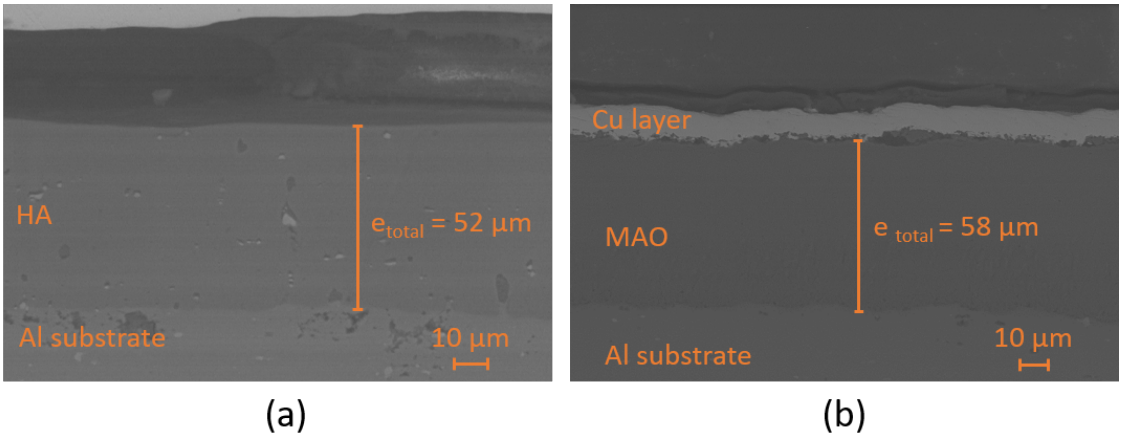

Figure 1: SEM-BSD micrograph of a HA coating (a) and a ground MAO coating cross-sections (b). A copper deposit was made to facilitate nanoindentation measurements.

Bruker's ContourX-500 profilometer was used to measure various parameters describing the HA and ground MAO surfaces. Measures are repeated five times to calculate the mean and standard deviations of each parameter. Four of them are presented in the Table 3. The average (Sa) and quadratic (Sq) surface roughnesses measured on the HA are about twice as low as those measured on the ground MAO. Both the HA and ground MAO surfaces have a kurtosis greater than 3. Their height distributions are therefore sharp on average with thick distribution tails. The kurtosis of

	Sa (µm)	Sq (µm)	S_{ku}	S_{sk}
HA	0.7 ± 0.05	1.1 ± 0.1	35 ± 12	−3.5 ± 0.7
g-MAO	1.5 ± 0.2	2.0 ± 0.2	17.8 ± 4	−1.6 ± 0.2

Table 3
Surface parameters describing HA and ground MAO coatings.

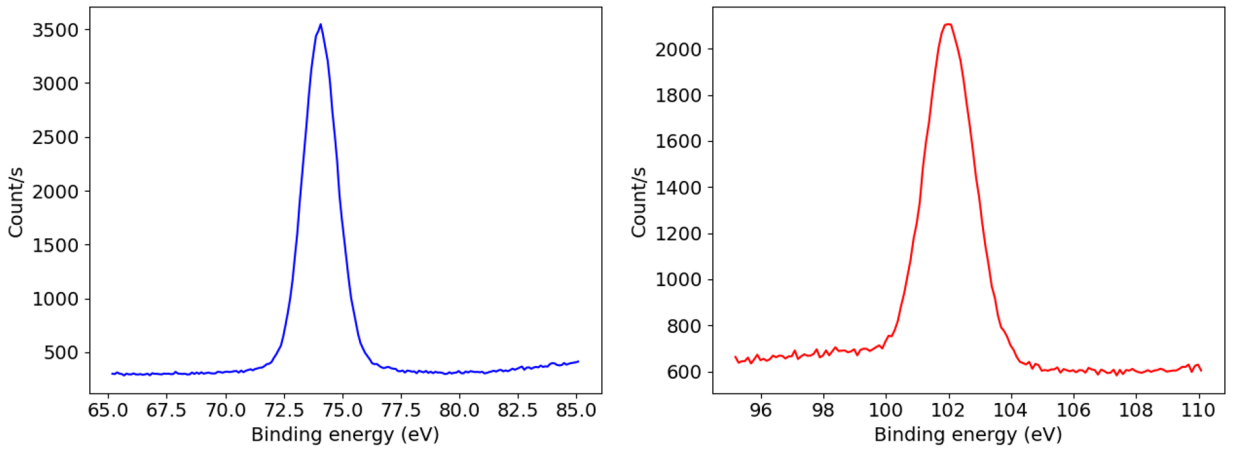

(a) (b)

Figure 2: XPS spectrum of Al2p (a) and Si2p binding energies measured on a MAO.

the HA surface is twice as high as that of ground MAO, the height distribution is higher on the HA surface than on the ground MAO. The skewness of the two coatings studied is less than zero. This is due to a shift in height distribution from the Gaussian above the baseline.

2.4. Physico-chemical analysis of the coatings

X-ray photoelectron spectrometry (XPS) provides quantitative information on the chemical elements present on the surface and their oxidation state. The spectra were recorded using a monochromatic Al Kα ($h\nu$ = 1486.6 eV) source on a ThermoScientific Kα system. The XPS spot size was about 400 µm. The pass energy was fixed at 30 eV with a step of 0.1 eV for core levels and 160 eV for surveys (step = 1 eV). The spectrometer energy calibration was done using the Au $4f_{7/2}$ (83.9 ± 0.1 eV) and Cu $2p_{3/2}$ (932.8 ± 0.1 eV) photoelectron lines. XPS spectra were recorded in direct mode N (Ec), and the background signal was removed using the Shirley method. The flood gun was used to neutralise charge effects on the top surface.

XPS analysis was carried out on the ground MAO coating. The main elements detected are O 1s (62.5%), Al 2p (27.5%) and Si 2p (8.4%). Other elements are minimally detected, such as Na 1s (0.8%), Mg 1s (0.5%) and K 2p (0.4%). The shift in binding energies (BE) measured on Al 2p (BE = 74.1 eV) testifies to the existence of the Al-O bond, confirmed by the one measured on Si 2p (BE = 102.0 eV) indicating the presence of the Si-O bond and the Al-Si-O bond [Figure 2] (35; 36).

A Philips X'Pert X-ray diffractometer (XRD) is used to analyse the composition of the crystalline phases present in the coatings. The wavelength used is the Cu Kα (λ = 1.54 nm). Working geometry is Bragg-Brentano ($\theta/2\theta$) with a scan angle between 20 and 160° and a measurement step of 0.02°. The diffractograms are analysed using Profex software. It is a graphical interface that allows performing Rietveld refinement with the program BGMN.

The analysis of the diffractogram obtained on HA [Figure 3.a] shows the presence of aluminium phase with lattice parameters $a = 0.406$ nm and a phase of aluminium hydroxide ($Al(OH)_3$) ($a = 0.512$ nm, $b = 0.507$ nm, $c = 0.510$ nm, $\alpha = 71°$, $\beta = 73°$, $\gamma = 59°$). About 91% of the crystalline part is from aluminium and 9% is from aluminium hydroxide. The shape of the diffractogram also indicates the existence of an amorphous phase in the layer. The ground MAO

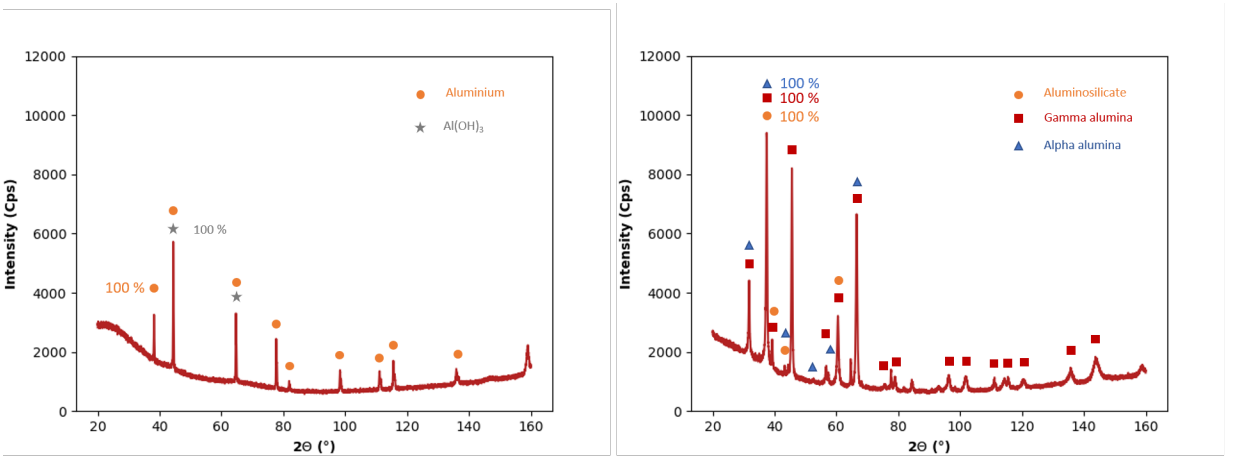

(a) (b)

Figure 3: Diffractograms obtained by XRD on an HA (a) and ground MAO (b) coatings.

	Al alloy	HA	g-MAO
Young's modulus (GPa)	92 ± 10	104 ± 4	330 ± 64
Hardness (GPa)	1.4 ± 0.3	6 ± 0.3	21 ± 4

Table 4
Average Young's modulus and Hardness measured on Al alloy, HA and ground MAO coating.

diffractogram shows that this coating consists of a gamma-alumina phase, alpha-alumina phase and an aluminosilicate phase [Figure 3.b]. About 73% of the crystalline phase is gamma-alumina of lattice parameter $a = 0.794$ nm. The aluminosilicate phase ($a = 0.519$ nm, $b = 0.898$ nm, $c = 0.744$ nm, $\alpha = 92.3°$, $\beta = 106°$, $\gamma = 89°$) represent 24% of the cristalline part. Finally, the alpha-alumina (corundum) phase represents 3% of the total crystalline phase and follows a rhombohedral arrangement with parameters $a = b = 0.476$ nm and $c = 1.297$ nm.

2.5. Mechanical properties

An XP nanoindenter from MTS is used to characterise the mechanical properties of the different coatings. Measurements are made in a cross-section to estimate the changes in properties as a function of the position in the layers. A Poisson's ratio of 0.3 is chosen to perform these calculations. Mappings are performed with five lines of 10 measurements. Measurements steps between each indentation are 10 µm in both x and y directions. The indentations were made in continuous stiffness measurement mode to a final depth of 500 nm. Hardness and stiffness are calculated between 200 nm and 450 nm depth. Mechanical properties are calculated from the average of the ten measurements made at each given distance from the substrate.

Nanoindentation mapping is performed on HA and ground MAO cross-section [Figure 4]. Young's modulus and hardness of the layers are given at different positions relative to the aluminium substrate. The average hardness and elastic modulus are gathered in Table 4. Hardness found on the HA coating is similar to the one found in other study (14). The highest hardness is 6.7 ± 0.2 GPa, and the maximum modulus is 113 ± 2 GPa. These are measured at 5 µm from the interface with the aluminium substrate. Then it decreases progressively as it approaches the surface. The highest mechanical properties are recorded in the ground MAO coating cross-section. Its hardness is 25 ± 5 GPa, and its maximum modulus is 430 ± 110 GPa at also 5 µm from the interface with the aluminium substrate. The trend curves for the two coatings show that the evolution of hardness and modulus are comparable within the layer. The further away from the interface with the substrate, the lower the mechanical property values. The modulus and hardness values found on the MAO coating are those that can be found in the literature (37; 38; 39). They are also comparable to measurements made on sintered α-alumina (39).

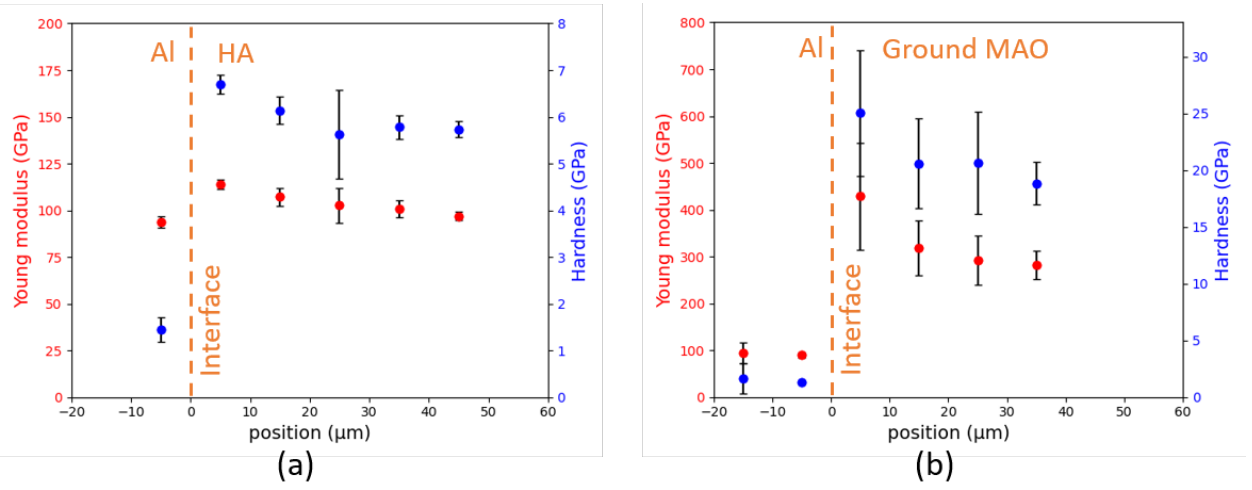

Figure 4: Young's modulus (E) and hardness (H) measured at different distances from the aluminium substrate in the HA (a) and ground MAO (b) coating.

Normal load (N)	Frequency (Hz)	Distance (mm)	Duration (s)	Temperature (°C)	Humidity Rate (%)
25 ± 0.5	5	10	1500	22 ± 3	55 ± 5

Table 5
Tribological test conditions.

3. Tribological test and wear behaviour

3.1. Friction measurement and energy dissipation

The UMT Tribolab ®produced by Bruker was performed in this study to evaluate the friction properties. It is a reciprocating linear tribometer used in a ball/plane contact geometry. The upper carriage is equipped with a DFH 50 G force transducer. Friction conditions were chosen from the standard ASTM G 133 (40) and are summarised in the Table 5. The balls used to implement this test are 99.5% pure polycrystalline alumina. Balls are 10 mm in diameter and finish grade 25. Hardness is 16.2 GPa, and Young's modulus is 370 GPa. Each friction test is repeated three times to estimate the repeatability.

Friction curve obtained on not coated aluminium alloy 5086 is first introduced [Figure 5]. It shows that a maximum of friction of 1.4 is reached at the beginning then it goes down to around 1 in an unstable manner until the end of the test. Secondly, those registered on HA and ground MAO coatings [Figure 6] including the averaged friction coefficient as well as the raw friction coefficients measured at 10 s and 750 s. The friction coefficient on the HA coating is irregular over the whole test. The friction coefficient (μ) is 0.73 ± 0.13 but oscillates in the range of $\mu = 1.1$, especially at the beginning of the test, and $\mu = 0.5$ during the significant part. Friction on the ground MAO increases with time and shows a disturbing pattern during the first 150 seconds. After that, the friction coefficient drops to a relatively stable value of about 0.90 until the end of the test. The mean value of the friction coefficient on ground MAO reaches 0.92 ± 0.06.

Dissipated energies (E_D) are calculated by multiplying the tangential force by the cumulative distance over the experiment. The proposed curves are derived from the average over the three tests. At the end of the test, an amount of 2.6 ± 0.02 kJ are dissipated during friction against the ground MAO and 1.7 ± 0.3 kJ against the HA coating [Figure 7]. This corresponds to an increase in energy dissipation of 53% with the ground MAO. The energy dissipated by the HA and ground MAO coatings is similar during the first 200 seconds. There is then a break in the slope of the energy dissipated by the HA reflecting a change in the accommodation mechanism inside the contact. The energy dispersion observed on the HA shows the increasing instability of dissipative phenomena between the three data sets.

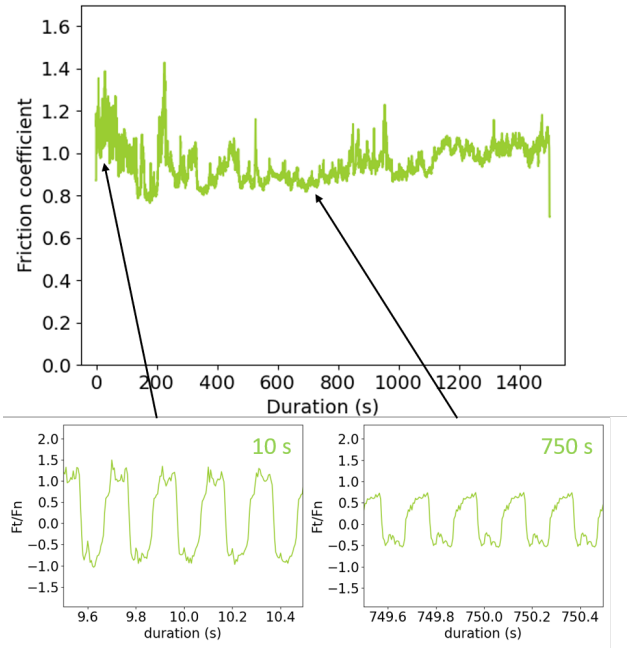

Figure 5: Friction coefficient between an alumina ball and an aluminium plane.

3.2. Wear evaluation and surface observations

The wear pattern of the HA coating is elliptical with two small deeper areas [Figure 8.a] and shows abrasion striations. The worn depth about 210 ± 25 µm which is much greater than that of the coating thickness [Table 6]. Furthermore, the width of the track on the plane is greater than that on the ball: the average radius of curvature in the trace is 3.7 ± 0.3 mm when the ball is 5 mm. This indicates a large amount of debris circulating in the contact and actively participating in the degradation of the plane. Images obtained on the ball show an addition of material to the surface without wear marks [Figure 8.b.c]. An HA wear rate of 6.7×10^{-4} $mm^3 \cdot N^{-1} \cdot m^{-1}$ is calculated from the worn volume measurement.

The ground MAO coating shows an oblong wear pattern with striation marks [Figure 9.a]. The areas of direction changes show deeper wear. The counter-face ball has striations characteristic of abrasion mechanisms [Figure 9.b.c]. The coating was worn down to a depth of about 15 ± 0.03 µm. The differences in track width between the ball and the plane and the average radius of curvature in the track of 12 ± 0.1 mm, which is about twice that of the ball, suggest again debris flow into the contact. The wear volume measurement on the ground MAO coating is 0.1 ± mm^3 which gives a calculated wear rate of 2.7×10^{-5} $mm^3 \cdot N^{-1} \cdot m^{-1}$ which is 13 times lower than that on HA coating. However, the ball having rubbed on the ground MAO coating shows a slight loss of material leading to a ball wear rate of 3.5×10^{-6} $mm^3 \cdot N^{-1} \cdot m^{-1}$, about 10 times lower than on the plane.

The total system wear rate, defined as the sum of the ball and plane wear rate, of the HA is approximately 6.7×10^{-4} $mm^3 \cdot N^{-1} \cdot m^{-1}$ while the one of the ground MAO is about 3.1×10^{-5} $mm^3 \cdot N^{-1} \cdot m^{-1}$.

SEM images of the HA planes after the tribological test are shown in Figure 10. The image at the direction change shows cracks, indicating that the coating has broken in this area [Figure 10.a]. The contact area is large, and the spread of material visible in the trace suggests adhesion phenomena and plastic deformation [Figure 10.b].

SEM observations on the ball that rubbed on the HA coating shown once again a deposit of material on the ball is 2.1 mm in width and 1.3 mm long with striations [Figure 11.a]. These observations suggest an adhesion mechanism of coating and substrate on the ball associated with abrasion phenomena on this deposited material. Typical thermal cracks can be observed below the tribofilm occurring at the opening of the contact at the end of the test, which causes a thermal shock fast enough to cause cracking [Figure 11.b].

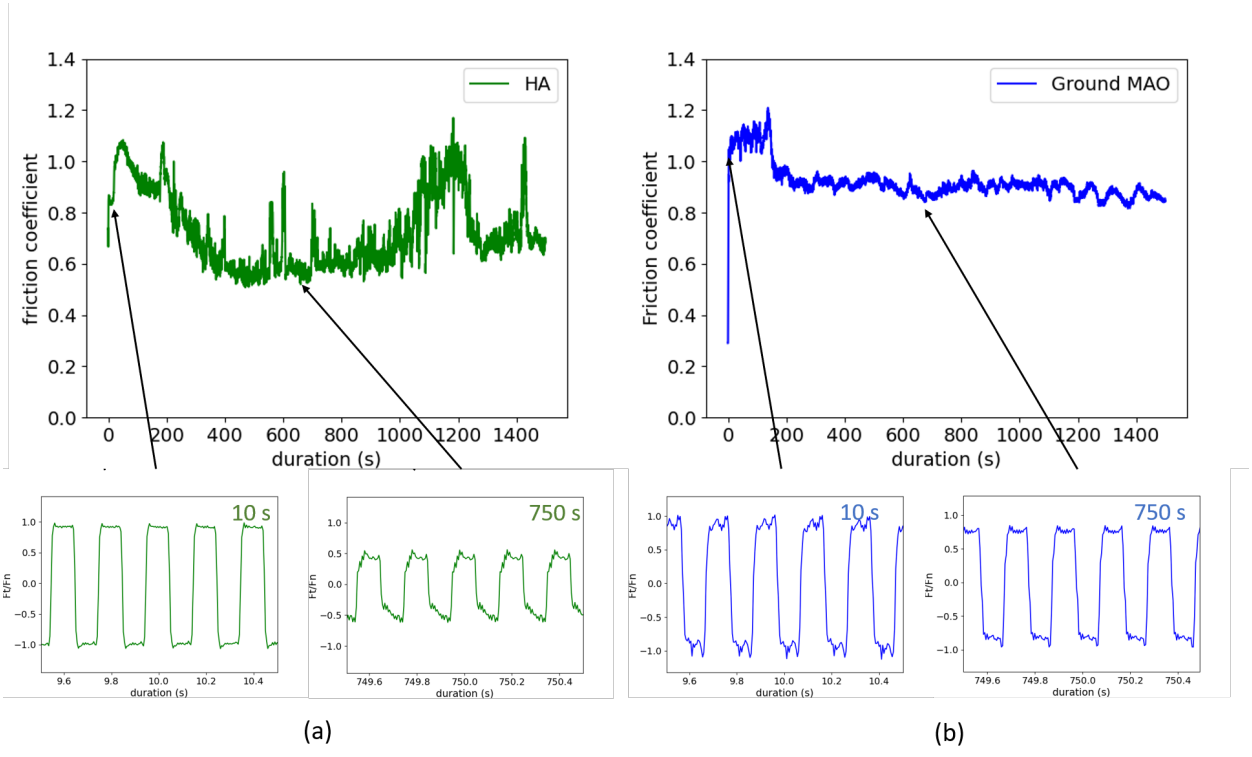

Figure 6: Curves of the average and raw friction coefficient obtained on HA (a) and ground MAO (b) coatings.

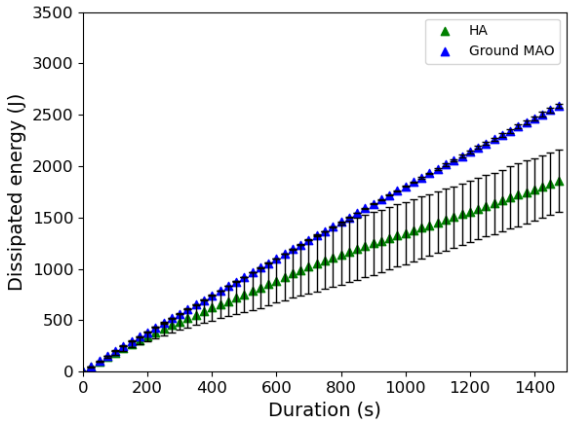

Figure 7: Cumulative dissipated energy calculated during the tribological test on an HA and ground MAO coatings.

SEM images of the ground MAO plane show that the contact area appears to be distributed over the entire wear pattern resulting in the distribution of forces on the whole surface between the ball and the plane where plastic deformation occurred 12.

190 The contact on the ball reveals a very homogeneous pattern with load-carrying areas where the material is smooth, suggesting a polishing effect of small debris [Figure 13].

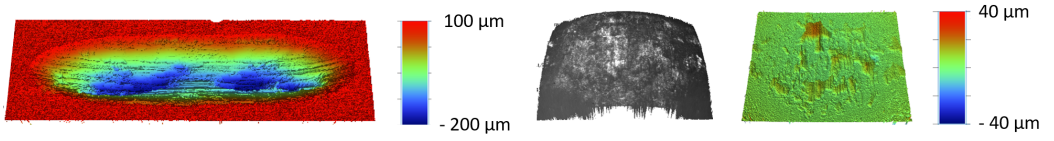

Figure 8: Optical profilometry measurements of the wear marks of the HA coating (a), topography of the ball with intensity overlay (b) and ball after a sphere removal (c) measured after friction test on HA coating after friction test. The deepest areas are in dark blue on the images while the highest areas are in red.

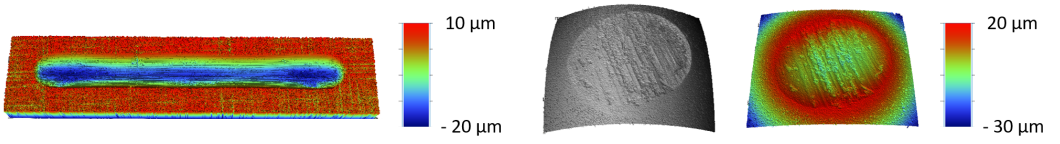

Figure 9: Optical profilometry measurements of the wear marks of the ground MAO coating (a), topography of the ball with intensity overlay (b) and ball after a sphere removal (c) measured after friction test on ground MAO coating after friction test. The deepest areas are in dark blue on the images while the highest areas are in red.

		HA	g-MAO
Plane	**Depth (µm)**	210 ± 25	15 ± 0.03
	Track width (mm)	2.4 ± 0.2	1.2 ± 0.1
	Wear volume (mm^3)	2.5 ± 0.3	0.1± 0.03
	Track width curvature (mm)	3,7 ± 0.3	12 ± 0.1
Ball	**Worn height(µm)**	−5 ± 3	25 ± 0.6
	Wear scar diameter (mm)	1.5 ± 0.2	1.2 ± 0.2
	Wear volume (mm^3)	−0,002 ± 0.001	0,013 ± 0.002

Table 6
Morphological parameters of the traces after tribological testing on HA and MAO coatings.

3.3. Discussion

The sliding of an alumina ball against the HA coating shows a friction coefficient lower than those measured on an aluminium substrate. The irregularity of the average friction curve obtained on the HA coating reflects the impossibility of setting up a stable third body within the contact. It is also noted from the mass loss measurements that the plane only participates in the generation of debris. Furthermore, the wear depth measurement shows that the entire coating has been degraded and that wear also deeply affects the substrate. However, the contact at the end of the test on the HA coating is not exactly that of the contact between the alumina ball and an aluminium substrate because the debris forms a tribofilm composed of a mixture of HA coating and aluminium substrate which contribute to reduce the tangential forces comparing to pure aluminium. Post mortem observations striations show abrasion of the coating down to the substrate and material deposits on the ball by adhesive mechanisms.

The friction between the alumina ball and the ground MAO coating takes place in two stages. During the first 150 seconds of the test, the tangential forces are very high, and the surfaces generate the first debris. The tribofilm is formed after these first 150 seconds and contributes to accommodating the velocity differences. One-third of the debris comes from the ball, while the other two-thirds come from the plane. After the 1500 s of testing, approximately 19% of the dense layer was worn away. Observations highlight abrasion and plastic deformation mechanisms on both the plane and the ball. Plastic deformation of debris is caused by the high compressive hydrostatic component generated during friction (41). Adhesive phenomena were also observed on the ball.

In addition, the kurtosis measured on the HA coating is twice as high as that measured on the ground MAO coating. This data reflects a morphology of the coating with thinner peaks and therefore, less resistance to sliding on the HA

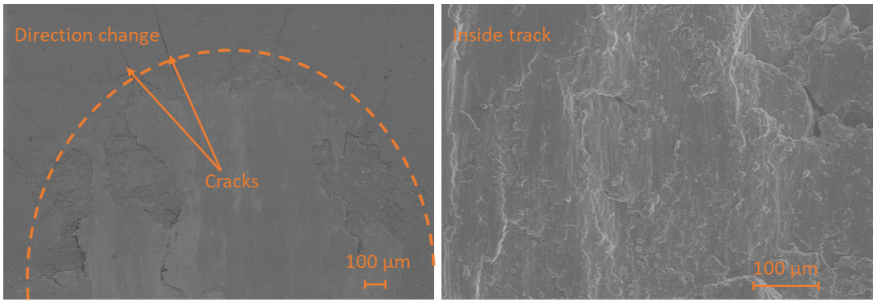

Figure 10: SEM images of the direction change (BSD) (a) and the inside of the track (SE) (b) of the HA plane after the tribological test.

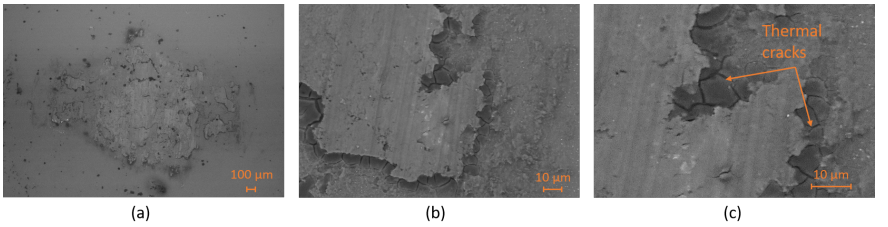

Figure 11: SEM-BSD images of the ball having rubbed against the HA coating (a), magnification in the friction area (b) and focus on the thermal cracks (c).

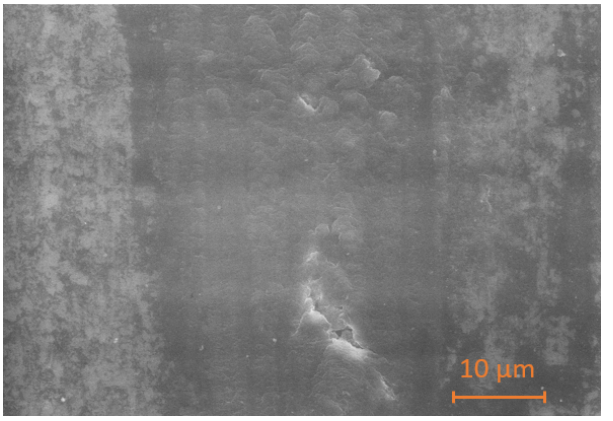

Figure 12: SEM-SE image inside the ground MAO track after the tribological test.

coating. Furthermore, the hardness of the ground MAO coating is about fifteen times higher than that measured on the HA coating and its modulus is about three times greater than that of the ground HA coating. The significant improvement in the mechanical properties of MAO compared to HA is due to the high concentration of gamma-alumina (73%) and the presence of alpha-alumina (3%). Finally, 0.7 kJ needs to be dissipated to wear 1 mm^3 in the HA tribocouple while 26 kJ is needed to remove the same amount of materials in the MAO tribocouple. These values show the dissipated energy divergences between the two coatings when the HA layer is consumed. It is much more difficult to create debris from coatings rather than from aluminium substrate. It can be explained by the stiffness differences.

The figure 14 proposes a comparison between HA coating and ground MAO coating wear behaviour by means of two schematic tribological circuits. The HA coating did not withstand the tribological test that was proposed in this study. This resulted in significant degradation of the substrate. The released metal particles formed an adhesive tribofilm

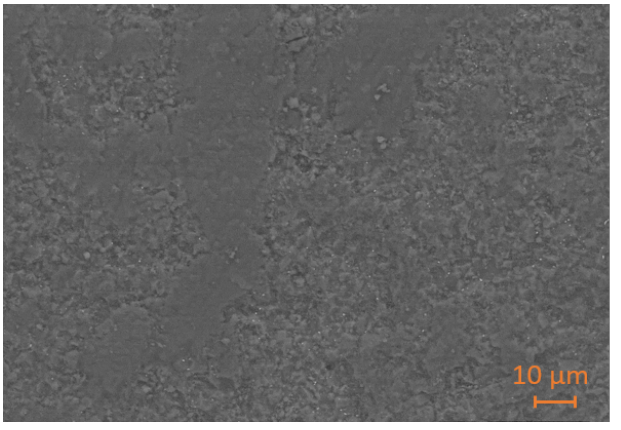

Figure 13: SEM-BSD images of the ball surface that have rubbed against the ground MAO coating.

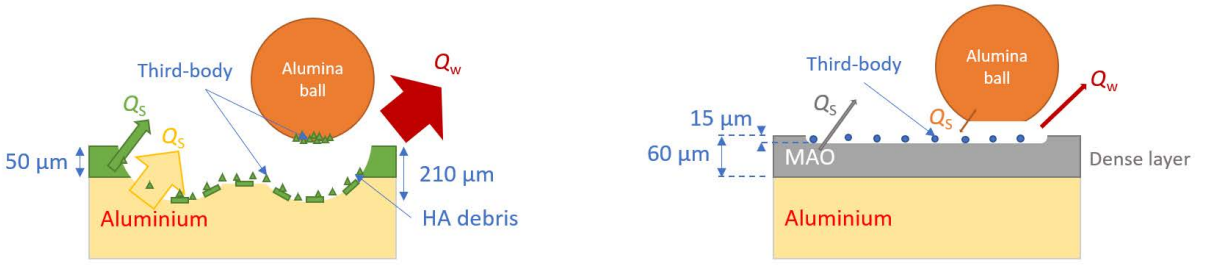

Figure 14: Tribological circuits obtained after the study of friction on an HA (a), a ground HA (b).

depositing on the ball. The energies dissipated were sufficiently large to cause thermal cracking on the ball when the contact was opened. Conversely, the ground coating, which no longer has a friable layer, shows the least worn at the end of the test.

4. Conclusions

Hard anodizing (HA) and micro-arc oxidation (MAO) coatings were deposited on a 5086 aluminium alloy. The rectified coating was diamond-ground to remove the entire friable layer. This study proposes to characterise and observe the differences in wear resistance of these coatings during a reciprocating linear tribological test in a ball/plane contact geometry. This work is the first study an industrially ground MAO surface which compare the tribological properties with those of HA. It also proposes a precise description of the local wear mechanisms and compare the main flows of matter acting in the contact (source and wear flows) for ground MAO and HA coatings under the same sliding conditions. They allow a comparison of the tribological behaviour of HA and ground MAO coatings under identical friction conditions. Some conclusions could be drawn:

- The chemical composition measurements show that the MAO coatings consist of aluminosilicates, alpha and gamma-alumina. The silicon added to the electrolyte is found in the totality of the layer in the form of aluminosilicate and amorphous silica.
- The hardness and elastic modulus MAO are about three times higher than those of the HA coating. It is also claimed that the mechanical properties of MAO increase as it gets closer to the substrate.
- The tribological test condition used in this study leads to the total degradation of the HA coating. In contrast, the ground MAO coating exhibits much higher performance. The mechanical processes of grinding allow both to

remove the well known friable layer from the MAO surface and decrease its roughness. The friction coefficient is directly related to the shear forces in the interface. At the beginning of the tribological test, this value depends on the interactions between the surfaces of the first two bodies. While during the rest of the test, it depends on the morphology and chemical nature of the third body. The total wear rate measured on the MAO coating tribocouple is 3.1 $\times$ 10^{-5} $mm^3 \cdot N^{-1} \cdot m^{-1}$ which is around 22 times lower than that obtained on the HA coating tribocouple. Also, adhesive strength explains why 0.7 kJ is needed to wear 1 mm^3 from the HA tribocouple while 26 kJ is necessary to remove the same amount of materials from the MAO tribocouple. Finally, it is found that different friction phases associated with large friction variations are observed on the HA while the friction is more stable on the MAO coating. These results shows that ground MAO is the best performing coating for improving the wear resistance of an aluminium surface.

Acknowledgments

Financial support was received from Occitanie country and ANRT academic/industry association in the context of a thesis of the University of Toulouse (n^o 2018/0988).

Appendix

CRediT authorship contribution statement

Louis Rodriguez: Methodology, Investigation, Writing - Original Draft, Writing - Review Editing, Visualization. **Aurélien Vieu:** Investigation. **Marion Balsarin:** Ressources, Review Editing, Project administration, Funding acquisition. **Philippe Combes:** Ressources, Review Editing, Project administration, Funding acquisition. **Joël Alexis:** Nanoindentation tests. **Jérôme Esvan:** XPS tests. **Samuel Lesko:** Optical profilometry tests. **Jean Denape:** Conceptualization, Validation, Writing - Review Editing. **Jean-Yves Paris:** Conceptualization, Validation, Writing - Review Editing. **Karl Delbé:** Conceptualization, Investigation, Validation, Writing - Original Draft, Writing - Review Editing, Supervision, Project administration, Funding acquisition.

References

[1] K. Holmberg, A. Erdemir, Influence of tribology on global energy consumption, costs and emissions, Friction 5 (3) (2017) 263–284. doi:10.1007/s40544-017-0183-5.

[2] C. J. Morgan, F. E. Brine, The Effect of Chromium Plating on the Fatigue Strength of Aluminium Alloy L65, Transactions of the IMF 47 (1) (1969) 77–79. doi:10.1080/00202967.1969.11870089.

[3] P. Kwolek, Hard anodic coatings on aluminum alloys, Advances in manufacturing science and technology 41 (3) (2017) 12.

[4] K. Du, X. Guo, Q. Guo, F. Wang, Y. Tian, A monolayer PEO coating on 2024 Al alloy by transient self-feedback control mode, Materials Letters 91 (2013) 45–49. doi:10.1016/j.matlet.2012.09.055.

[5] N. Godja, N. Kiss, C. Löcker, A. Schindel, A. Gavrilovic, J. Wosik, R. Mann, J. Wendrinsky, A. Merstallinger, G. Nauer, Preparation and characterization of spark-anodized Al-alloys: Physical, chemical and tribological properties, Tribology International 43 (7) (2010) 1253–1261. doi:10.1016/j.triboint.2010.01.007.

[6] A. L. Yerokhin, L. O. Snizhko, N. L. Gurevina, A. Leyland, A. Pilkington, A. Matthews, Discharge characterization in plasma electrolytic oxidation of aluminium, Journal of Physics D: Applied Physics 36 (17) (2003) 2110–2120. doi:10.1088/0022-3727/36/17/314.

[7] F. Di Quarto, S. Piazza, C. Sunseri, Breakdown Phenomena During the Growth of Anodic Oxide Films on Zirconium Metal: Influence of Experimental Parameters on Electrical and Mechanical Breakdown, J. Electrochem. Soc. 131 (12) (1984) 2901–2906. doi:10.1149/1.2115439.

[8] S. Ikonopisov, Theory of electrical breakdown during formation of barrier anodic films, Electrochimica Acta 22 (10) (1977) 1077–1082. doi:10.1016/0013-4686(77)80042-X.

[9] S. Moon, Y. Jeong, Generation mechanism of microdischarges during plasma electrolytic oxidation of Al in aqueous solutions, Corrosion Science 51 (7) (2009) 1506–1512. doi:10.1016/j.corsci.2008.10.039.

[10] A. Yerokhin, X. Nie, A. Leyland, A. Matthews, S. Dowey, Plasma electrolysis for surface engineering, Surface and Coatings Technology 122 (2-3) (1999) 73–93. doi:10.1016/S0257-8972(99)00441-7.

[11] S. Fidan, F. Muhaffel, M. Riool, G. Cempura, L. de Boer, S. Zaat, A. C. Filemonowicz, H. Cimenoglu, Fabrication of oxide layer on zirconium by micro-arc oxidation: Structural and antimicrobial characteristics, Materials Science and Engineering: C 71 (2017) 565–569. doi:10.1016/j.msec.2016.11.035.

[12] A. Dey, R. Rani, H. K. Thota, A. K. Sharma, P. Bandyopadhyay, A. K. Mukhopadhyay, Microstructural, corrosion and nanomechanical behaviour of ceramic coatings developed on magnesium AZ31 alloy by micro arc oxidation, Ceramics International 39 (3) (2013) 3313–3320. doi:10.1016/j.ceramint.2012.10.020.

[13] T. Teh, A. Berkani, S. Mato, P. Skeldon, G. Thompson, H. Habazaki, K. Shimizu, Initial stages of plasma electrolytic oxidation of titanium, Corrosion Science 45 (12) (2003) 2757–2768. doi:10.1016/S0010-938X(03)00101-X.

[14] U. Malayoglu, K. C. Tekin, U. Malayoglu, S. Shrestha, An investigation into the mechanical and tribological properties of plasma electrolytic oxidation and hard-anodized coatings on 6082 aluminum alloy, Materials Science and Engineering: A 528 (24) (2011) 7451–7460. doi:10.1016/j.msea.2011.06.032.

[15] J. Tian, Z. Luo, S. Qi, X. Sun, Structure and antiwear behavior of micro-arc oxidized coatings on aluminum alloy, Surface and Coatings Technology 154 (1) (2002) 1–7. doi:10.1016/S0257-8972(01)01671-1.

[16] X. Nie, A. Leyland, H. Song, A. Yerokhin, S. Dowey, A. Matthews, Thickness effects on the mechanical properties of micro-arc discharge oxide coatings on aluminium alloys, Surface and Coatings Technology 116–119 (1999) 1055–1060. doi:10.1016/S0257-8972(99)00089-4.

[17] X. Lv, L. Cao, Y. Wan, T. Xu, Effect of different electrolytes in micro-arc oxidation on corrosion and tribological performance of 7075 aluminum alloy, Mater. Res. Express 6 (8) (2019) 086421. doi:10.1088/2053-1591/ab1da5.

[18] N. Xiang, R.-G. Song, J.-J. Zhuang, R.-X. Song, X.-Y. Lu, X.-P. Su, Effects of current density on microstructure and properties of plasma electrolytic oxidation ceramic coatings formed on 6063 aluminum alloy, Transactions of Nonferrous Metals Society of China 26 (3) (2016) 806–813. doi:10.1016/S1003-6326(16)64171-7.

[19] P. Yi, W. Yue, J. Liang, B. Hou, J. Sun, Y. Gu, J. Liu, Effects of nanocrystallized layer on the tribological properties of micro-arc oxidation coatings on 2618 aluminum alloy under high temperatures, Int J Adv Manuf Technol 96 (5-8) (2018) 1635–1646. doi:10.1007/s00170-017-0831-y.

[20] C. Wang, J. Chen, J. He, J. Jiang, Q. Zhang, Effect of electrolyte concentration on the tribological performance of MAO coatings on aluminum alloys, Front. Chem. Sci. Eng.doi:10.1007/s11705-019-1909-x.

[21] E. Arslan, Y. Totik, E. Demirci, Y. Vangolu, A. Alsaran, I. Efeoglu, High temperature wear behavior of aluminum oxide layers produced by AC micro arc oxidation, Surface and Coatings Technology 204 (6-7) (2009) 829–833. doi:10.1016/j.surfcoat.2009.09.057.

[22] N. Barati, E. Meletis, F. Golestani Fard, A. Yerokhin, S. Rastegari, M. Faghihi-Sani, Al_2O_3/ZrO_2 nanostructured coatings using DC plasma electrolytic oxidation to improve tribological properties of Al substrates, Applied Surface Science 356 (2015) 927–934. doi:10.1016/j.apsusc.2015.08.188.

[23] A. Polat, M. Makaraci, M. Usta, Influence of sodium silicate concentration on structural and tribological properties of microarc oxidation coatings on 2017A aluminum alloy substrate, Journal of Alloys and Compounds 504 (2) (2010) 519–526. doi:10.1016/j.jallcom.2010.06.008.

[24] G. Sabatini, L. Ceschini, C. Martini, J. Williams, I. Hutchings, Improving sliding and abrasive wear behaviour of cast A356 and wrought AA7075 aluminium alloys by plasma electrolytic oxidation, Materials & Design 31 (2) (2010) 816–828. doi:10.1016/j.matdes.2009.07.053.

[25] X. Nie, E. I. Meletis, J. C. Jiang, A. Leyland, A. L. Yerokhin, A. Matthews, Abrasive wear/corrosion properties and TEM analysis of Al_2O_3 coatings fabricated using plasma electrolysis, Surface and Coatings Technology (2002) 7.

[26] M. Godet, The third-body approach: A mechanical view of wear, Wear 100 (1) (1984) 437–452. doi:10.1016/0043-1648(84)90025-5.

[27] Y. Berthier, M. Godet, M. Brendle, Velocity Accommodation in Friction, Tribology Transactions 32 (4) (1989) 490–496. doi:10.1080/10402008908981917.

[28] J. Denape, Third Body Concept and Wear Particle Behavior in Dry Friction Sliding Conditions, KEM 640 (2015) 1–12. doi:10.4028/www.scientific.net/KEM.640.1.

[29] L. R. Krishna, A. S. Purnima, G. Sundararajan, A comparative study of tribological behavior of microarc oxidation and hard-anodized coatings, Wear 261 (10) (2006) 1095–1101. doi:10.1016/j.wear.2006.02.002.

[30] X.-J. Li, M. Zhang, S. Wen, X. Mao, W.-G. Huo, Y.-Y. Guo, Y.-X. Wang, Microstructure and wear resistance of micro-arc oxidation ceramic coatings prepared on 2A50 aluminum alloys, Surface and Coatings Technology 394 (2020) 125853. doi:10.1016/j.surfcoat.2020.125853.

[31] NF EN 515 : Aluminium et alliages d'aluminium - Produits corroyés - Désignation des états métallurgiques, Standard, Association Française de Normalisation (AFNOR) (Apr. 2017).

[32] NF EN 2693:2005-11 - Alliage d'aluminium AL - P5086 H111 - Tôles et bandes - 0,3 mm $\leq$ a $\leq$ 6 mm. (Nov. 2005).

[33] Comité Technique CEN/TC132«Aluminium et alliages d'aluminium», NF EN 485-2 + A1 : 2018-10 - Aluminium et alliages d'aluminium - Tôles, bandes et tôles épaisses - Partie 2: Caractéristiques mécaniques (Oct. 2018).

[34] J. Beauvir, Procédé électrolytique d'oxydation pour l'obtention d'un revêtement céramique à la surface d'un métal (Apr. 2001).

[35] A. Roy Chowdhuri, C. Takoudis, Investigation of the aluminum oxide/Si(100) interface formed by chemical vapor deposition, Thin Solid Films 446 (1) (2004) 155–159. doi:10.1016/S0040-6090(03)01311-7.

[36] F. Monfort, A. Berkani, E. Matykina, P. Skeldon, G. Thompson, H. Habazaki, K. Shimizu, Development of anodic coatings on aluminium under sparking conditions in silicate electrolyte, Corrosion Science 49 (2) (2007) 672–693. doi:10.1016/j.corsci.2006.05.046.

[37] X. Shi-Gang, S. Li-Xin, Z. Rong-Gen, H. Xing-Fang, Properties of aluminium oxide coating on aluminium alloy produced by micro-arc oxidation, Surface and Coatings Technology 199 (2-3) (2005) 184–188. doi:10.1016/j.surfcoat.2004.11.044.

[38] W. Xue, C. Wang, Z. Deng, R. Chen, Y. Li, T. Zhang, Evaluation of the mechanical properties of microarc oxidation coatings and 2024 aluminium alloy substrate, J. Phys.: Condens. Matter 14 (44) (2002) 10947–10952. doi:10.1088/0953-8984/14/44/407.

[39] J. Curran, T. Clyne, Thermo-physical properties of plasma electrolytic oxide coatings on aluminium, Surface and Coatings Technology 199 (2-3) (2005) 168–176. doi:10.1016/j.surfcoat.2004.09.037.

[40] G02 Committee, ASTM G 133 - Test Method for Linearly Reciprocating Ball-on-Flat Sliding Wear, Norme, ASTM International (2010). doi:10.1520/G0133-05R10.

[41] B. J. Hockey, Plastic Deformation of Aluminum Oxide by Indentation and Abrasion, J American Ceramic Society 54 (5) (1971) 223–231. doi:10.1111/j.1151-2916.1971.tb12277.x.